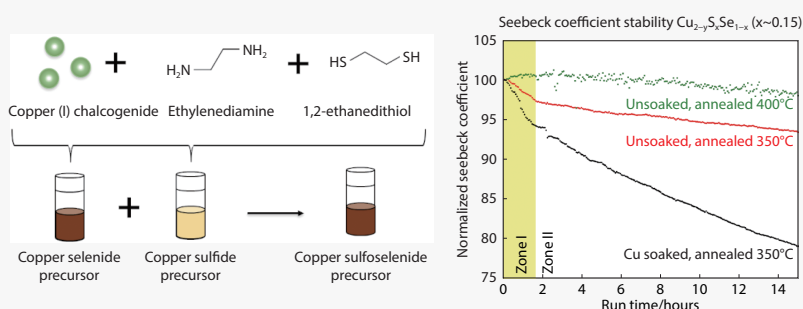


# Harnessing high power factors with enhanced stability in heavy metal-free solution-processed thermoelectric copper sulfoselenide thin films

Håvard Mølneås, Michael R. Scimeca and Ayaskanta Sahu<sup>\*ID</sup>

Thermoelectric devices have the potential to recover waste heat from inefficient energy conversion processes. State-of-the-art thermoelectrics demonstrate low efficiency and incorporate materials containing rare and toxic elements. In this regard, p-type copper selenide ( $\text{Cu}_2\text{Se}$ ) has been identified as a promising and environmentally benign alternative. Unfortunately, the high diffusivity of liquid-like copper ions results in structural instability and performance degradation during operation, especially at moderate to high temperatures above 200 °C. Sulfur substitution has been utilized in melt-annealed samples to improve the stability of  $\text{Cu}_2\text{Se}$  during operation, however this fabrication process is energy intensive and does not allow for use of flexible substrates. In this work, we report a solution-based direct thin film route to tune carrier concentration in copper sulfoselenide ( $\text{Cu}_{2-y}\text{S}_x\text{Se}_{1-x}$ ) thin films by controlling sulfur content and degree of copper saturation. We observe that improved thermoelectric performance through copper saturation in nominally copper-deficient  $\text{Cu}_{2-y}\text{Se}$  films comes at a huge cost, with significantly reduced material stability due to enhanced copper migration resulting in severe degradation of the thermopower. Circumventing copper saturation, we show that controlled sulfur addition and tuning of annealing temperature has a synergistic effect, resulting in improved stability of the thermoelectric properties during continuous operation for mildly copper-deficient films while sustaining a high power factor of  $800 \mu\text{W m}^{-1} \text{K}^{-2}$  at room temperature. Our results demonstrate a pathway for generating high performance solution processed thermoelectric devices with flexible form factors, and reinforce the case for  $\text{Cu}_{2-y}\text{S}_x\text{Se}_{1-x}$  thin films as a heavy metal-free alternative for scavenging low grade waste heat.



Most energy conversion technologies developed to meet exponentially increasing energy demands still have low efficiencies.<sup>[1,2]</sup> In addition, due to limited availability of energy recovery technologies, a huge fraction of usable energy is wasted. Thermoelectric devices can harness this waste heat and convert it into electricity without having any moving parts, giving off noise or emitting greenhouse gasses.<sup>[3,4]</sup> The durability and ease of scalability of thermoelectric materials make them very appealing for energy harvesting, however, the efficiency of thermoelectric devices is still low, and state of the art thermoelectric materials such as bismuth telluride ( $\text{Bi}_2\text{Te}_3$ ), antimony telluride ( $\text{Sb}_2\text{Te}_3$ ) and lead telluride ( $\text{PbTe}$ ) contain toxic and heavy elements which need to be handled safely during manufacture and recycling.

Department of Chemical and Biomolecular Engineering, New York University, Tandon School of Engineering, 6 MetroTech Center, Brooklyn, New York 11201, United States

\* Corresponding author, E-mail: [asahu@nyu.edu](mailto:asahu@nyu.edu)

Received 23 May 2022; Accepted 22 September 2022; Published online

The figure of merit for thermoelectric materials is typically reported as the  $ZT$  value, calculated as  $ZT = \frac{\sigma\alpha^2}{\kappa}T$ , where  $\sigma$  is the electrical conductivity,  $\kappa$  is thermal conductivity,  $T$  is temperature and  $\alpha$  is the Seebeck coefficient, defined as the negative slope of the open circuit voltage per temperature gradient,  $\frac{-dV_{oc}}{dT}$ . Optimizing the  $ZT$  for thermoelectric materials is a competition between conflicting materials properties, as increased carrier concentration typically results in higher electrical conductivity and higher thermal conductivity, while reducing the Seebeck coefficient. Therefore, one often aims to maximize the power factor,  $PF = \sigma\alpha^2$ , through controlling the charge carrier density while employing different strategies to reduce the thermal conductivity. This includes controlling grain sizes, relying on nanostructures or using 'phonon-liquid electron-crystals'.<sup>[4,5]</sup>

An environmentally friendly alternative to the state-of-the-art thermoelectric materials is copper selenide ( $\text{Cu}_2\text{Se}$ ) which has been studied since the 1960s due to its high performance, low raw material cost and favorable environmental

footprint.<sup>[6,7]</sup> The cubic  $\beta$ -Cu<sub>2-y</sub>Se phase has been shown to possess more favorable thermoelectric properties than other Cu-Se phases.<sup>[8]</sup> However, due to stability issues, pure Cu<sub>2</sub>Se struggled to compete with other energy conversion technologies and was abandoned. This instability is manifested due to the liquid-like behavior of cations such as copper(I) (Cu<sup>+</sup>), silver(I) (Ag<sup>+</sup>) and zinc(II) (Zn<sup>2+</sup>). While showing high thermoelectric performance, decent electrical transport properties and ultralow lattice thermal conductivity due to direct or indirect scattering of phonons,<sup>[9]</sup> cation diffusion under external temperature or current gradients leads to metal deposition and subsequent performance and material degradation.<sup>[10]</sup> Qiu et al.<sup>[11]</sup> studied this phenomenon and claimed that this is due to a critical chemical potential difference, which can be manifested through an expression for a critical voltage difference at which Cu deposition will occur:

$$V_C = -\frac{RT}{F} \left( \arcsin\left(\frac{\delta_c}{2\sqrt{K_e}}\right) - \arcsin\left(\frac{2\delta - \delta_c}{2\sqrt{K_e}}\right) \right) \quad (1)$$

In equation (1),  $V_C$  is the critical voltage,  $R$  is the gas constant,  $T$  is the temperature,  $F$  is Faraday's constant,  $\delta$  is the off-stoichiometry of Cu<sub>2-y</sub>Se,  $\delta_c$  is the critical off-stoichiometry and  $K_e$  is the equilibrium constant for electrons and holes.  $V_C$  can be measured experimentally as a function of applied electric current or temperature gradients.

Several strategies have been proposed to control the stability of Cu<sub>2</sub>Se: Qiu et al.<sup>[11]</sup> introduced electrically conductive ion-blocking interfaces such as grain boundaries and secondary phases to limit ion movement. Yang et al.<sup>[6]</sup> incorporated bismuth copper oxyselenide (BiCuSeO) nanoparticles (NPs) into the Cu<sub>2</sub>Se matrix, creating an ion-modulated interfacial electrostatic field blocking long-range migration of Cu<sup>+</sup> ions. While the incorporation of NPs did reduce the power factor from 800 to 700  $\mu\text{W m}^{-1} \text{K}^{-2}$ , the BiCuSeO NPs simultaneously served as phonon scattering structures reducing the thermal conductivity, thus improving the overall performance of the thermoelectric. In a similar manner, Farooq et al. introduced 5-15 wt% copper sulfide (Cu<sub>2</sub>S) NPs into the Cu<sub>2-y</sub>Se matrix and reduced the power factor from ~600 to ~280 – 490  $\mu\text{W m}^{-1} \text{K}^{-2}$ ,<sup>[12]</sup> however the overall thermoelectric performance was improved due to reduced thermal conductivity.

Introducing single foreign elements into the crystal structure has also been attempted with varying degree of success. Although improving performance slightly, doping with elemental tin (Sn) and lithium (Li) did not produce clear improvements in stability.<sup>[13,14]</sup> Mao et al.<sup>[9]</sup> and Zhao et al.<sup>[15–17]</sup> explored sulfur (S) alloying as a route to Cu<sub>2</sub>Se stabilization, and showed that for melt-annealed samples, a slight Cu deficiency (Cu:Se ratio 1.96:1 as compared to stoichiometric 2:1) in combination with up to 20% selenium (Se) substitution with S was favorable both with regards to performance as well as material stability. Zhao et al.<sup>[15]</sup> improved the power factor from ~750  $\mu\text{W m}^{-1} \text{K}^{-2}$  for Cu<sub>2</sub>Se to ~1125  $\mu\text{W m}^{-1} \text{K}^{-2}$  for Cu<sub>2</sub>S<sub>0.06</sub>Se<sub>0.94</sub> at 300 K. Mao et al.<sup>[9]</sup> report power factors in the range ~600  $\mu\text{W m}^{-1} \text{K}^{-2}$  for Cu<sub>2-y</sub>Se and Cu<sub>2-y</sub>S<sub>x</sub>Se<sub>1-x</sub> and 800 – 1000  $\mu\text{W m}^{-1} \text{K}^{-2}$  for Cu<sub>2</sub>S<sub>x</sub>Se<sub>1-x</sub> at 300 K. Exploring the sulfur-rich regime, Xiang et al.<sup>[18]</sup> added Se to Cu<sub>2-y</sub>S and improved the power factor at 325 K from ~200  $\mu\text{W m}^{-1} \text{K}^{-2}$  for Cu<sub>1.8</sub>S to ~450  $\mu\text{W m}^{-1} \text{K}^{-2}$  for Cu<sub>1.8</sub>S<sub>0.8</sub>Se<sub>0.2</sub> while reducing material decomposition.

Relying on a melting-annealing process for device preparation limits the use of flexible substrates and hinders smooth incorporation of thermoelectric materials into low grade heat harvesting applications requiring curved shapes, such as around exhaust pipes or in clothing. Perez-Taborda et al.<sup>[19]</sup> achieved an impressive room temperature power factor of 1100  $\mu\text{W m}^{-1} \text{K}^{-2}$  through pulsed hybrid reactive magnetron sputtering on polyimide tape. A room temperature power factor of 844  $\mu\text{W m}^{-1} \text{K}^{-2}$  was obtained by Wang et al.<sup>[20]</sup> utilizing pulsed laser deposition to grow epitaxial Cu<sub>2</sub>Se films while keeping the substrate temperature below 300 °C. Lu et al.<sup>[21]</sup> fabricated flexible nanocomposite poly(3,4-ethylenedioxythiophene):poly(styrenesulfonate)(PEDOT:PSS)/Cu<sub>x</sub>Se<sub>y</sub> films on nylon substrates through vacuum assisted filtration and cold-pressing and measured a power factor of 270  $\mu\text{W m}^{-1} \text{K}^{-2}$ . Mallick et al.<sup>[22]</sup> explored S substitution in Cu<sub>2-y</sub>Se on flexible substrates through a ball milling, printing and sintering process, but their material only reached a power factor of ~250  $\mu\text{W m}^{-1} \text{K}^{-2}$  for 10 at% S substitution at 300 K. Lin et al.<sup>[23]</sup> showed that direct thin film deposition of Cu<sub>2</sub>Se based on a route inspired by Webber and Brutchey<sup>[24]</sup> produces films with decent thermoelectric performance (power factors 100 – 200  $\mu\text{W m}^{-1} \text{K}^{-2}$  at room temperature) on rigid and flexible substrates, while Ma et al.<sup>[25]</sup> performed initial experiments with S and silver (Ag) doping of Cu<sub>2</sub>Se direct thin films, achieving power factors around ~100  $\mu\text{W m}^{-1} \text{K}^{-2}$ . Our group later showed that this direct film route allows for straight-forward Cu saturation and/or cation exchange while still allowing for integration with flexible substrates.<sup>[26,27]</sup> While most of these previous direct thin film studies concentrated on improving the power factor with impressive numbers reported (653  $\mu\text{W m}^{-1} \text{K}^{-2}$  at room temperature ref. Scimeca et al.<sup>[26]</sup>), the devices showed slow degradation of the thermopower over time (11.4 % degradation of Seebeck coefficient in 21.7 hours). Hence, the focus now needs to shift to the stability of these material systems in devices in order to render them feasible for commercial applications.

In this work, we explore Se substitution by S in unsaturated and Cu soaked Cu<sub>2</sub>Se films by the direct thin film route introduced above in order to establish a straightforward route to stable and flexible Cu<sub>2-y</sub>S<sub>x</sub>Se<sub>1-x</sub> thermoelectric devices capable of scavenging low grade waste heat at room temperature. The thin films were characterized using a range of techniques, including X-ray diffraction (XRD), energy-dispersive X-ray spectroscopy (EDS), X-ray photoelectron spectroscopy (XPS) and absorbance measurements in the visible, near infrared and short-wave infrared. The electrical conductivity of the films was determined, and static and transient Seebeck coefficient measurements were performed to evaluate the stability of these films. Our study shows that this direct thin film technique is suitable for tuning the carrier concentration in Cu<sub>2-y</sub>S<sub>x</sub>Se<sub>1-x</sub> films through varying S content and Cu saturation. The addition of S improves the stability of the thin film over time, while sustaining the high power factor. Cu saturation improves performance, however it is not favorable for stability, and we found that S addition combined with optimization of the annealing temperature is a better strategy for achieving stable Cu<sub>2-y</sub>S<sub>x</sub>Se<sub>1-x</sub> films with high thermoelectric performance at room temperature.

## Materials and methods

### Chemicals and substrates

Copper (I) selenide ( $\text{Cu}_2\text{Se}$ , 99.95%), copper (I) sulfide ( $\text{Cu}_2\text{S}$ , anhydrous, 99.99%) ethylenediamine ( $\text{H}_2\text{NCH}_2\text{CH}_2\text{NH}_2$ , synthesis grade) and 1,2-ethanedithiol ( $\text{HSCH}_2\text{CH}_2\text{SH}$ , >90%) were purchased from Sigma-Aldrich. Acetone ( $\text{H}_3\text{CCOCH}_3$ , reagent grade), isopropyl alcohol ( $(\text{CH}_3)_2\text{CHOH}$ , reagent grade) and methanol ( $\text{CH}_3\text{OH}$ , reagent grade) were purchased from Greenfield Global. Tetrakis(acetonitrile)copper(I)hexafluorophosphate was purchased from TCI. All the chemicals were used as received without further purification.

Glass substrates, 9.5 mm x 9.5 mm, and 0.2 mm thick, were purchased from Thin Film Devices. Substrates were cleaned by sonication in acetone, isopropanol and methanol (10 minutes in each solvent) and plasma treated for 20 minutes.

### Thin film fabrication

Unsaturated and Cu soaked  $\text{Cu}_{2-y}\text{S}_x\text{Se}_{1-x}$  direct thin films with different amounts of S were fabricated in accordance with previous work (Scheme 1).<sup>[25,26]</sup> Utilizing the thiol-amine approach<sup>[24]</sup>, smooth and continuous  $\text{Cu}_{2-y}\text{S}_x\text{Se}_{1-x}$  films of average thickness  $61 \text{ nm} \pm 7 \text{ nm}$  were fabricated by spin coating mixed  $\text{Cu}_2\text{Se}$ - $\text{Cu}_2\text{S}$  inks onto clean glass substrates, followed by annealing on a hot plate or in an oven at  $350^\circ\text{C}$  or  $400^\circ\text{C}$ , respectively. Ramping rate was  $50^\circ\text{C}/5 \text{ min}$ , and holding time at elevated temperature was 1 hour. The mixed inks consisted of predetermined ratios of  $\text{Cu}_2\text{Se}$  and  $\text{Cu}_2\text{S}$  inks, fabricated by dissolving 100 mg  $\text{Cu}_2\text{Se}$  or 77.2 mg  $\text{Cu}_2\text{S}$  in 2 mL ethylenediamine (EN) and 0.2 mL 1,2-ethanedithiol (EDT). A subset of samples were soaked in 0.05 M tetrakis(acetonitrile)

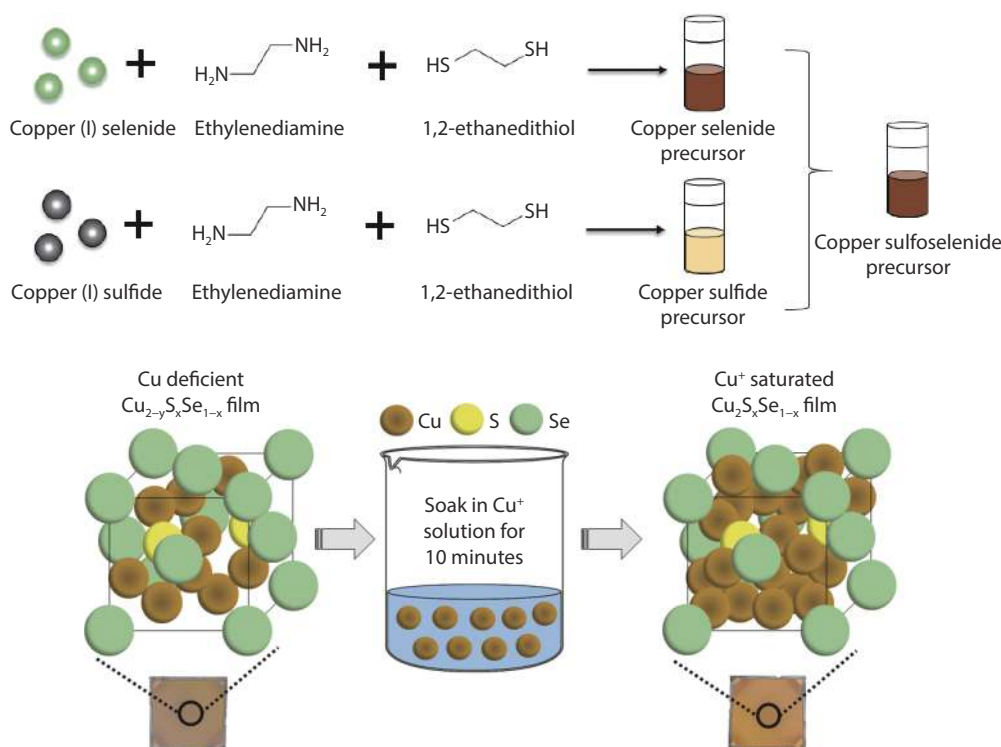
copper(I)hexafluorophosphate solution in methanol for 10 minutes, followed by 5 seconds rinse in methanol and drying on a hot plate at  $70^\circ\text{C}$  for 2 min. 60 nm gold (Au) electrodes were deposited on all four corners of each sample through thermal evaporation. All fabrication steps took place in a nitrogen filled glove box.

### Characterization

Electrical conductivity was measured via the standard 4-probe van-der-Pauw method and Seebeck measurements were performed on a homemade setup using small Peltier units (CUI Inc.) to provide various temperature gradients, both in a nitrogen filled glovebox. A Labview program was used with Keithley 2400 source meters and Keithley 2000 multimeters to provide current sources and measure voltages.

Visible, near infrared and short-wave infrared absorption spectra were measured on an Agilent Cary 5000 UV-Vis spectrophotometer in air. XRD spectra were acquired using a Bruker AXS D8 Discover GADDS instrument. S:Se ratios were determined through energy-dispersive X-ray spectroscopy using a Zeiss Gemini Ultra-55 Analytical Field Emission Scanning Electron Microscope (SEM). Film thickness was determined using a Veeco Dektak 150 profilometer.

XPS for examining Cu, Se, and S edges was performed using a Physical Electronics Versaprobe II XPS. An Al  $K\alpha$  source set to 49.4 W and 1.487 keV (250 meV resolution) with a 200  $\mu\text{m}$  beam diameter was used to collect spectra. For survey pass, the energy was set to 117.40 eV, while the elemental pass energies were set to 29.35 eV. Spectra were corrected by shifting the C1s peak to 284.8 eV prior to analysis.



**Scheme 1** Preparation of  $\text{Cu}_{2-y}\text{S}_x\text{Se}_{1-x}$  precursor and  $\text{Cu}^+$  saturation of  $\text{Cu}_{2-y}\text{S}_x\text{Se}_{1-x}$  films.<sup>[26]</sup> Copyright 2019, American Chemical Society.

## Results and Discussion

### Structure

XRD spectra (Figure S1 in the Supplemental Information, SI) show the existence of unsaturated  $\text{Cu}_{2-y}\text{S}_x\text{Se}_{1-x}$  annealed at 350 °C as cubic  $\text{Cu}_{2-y}\text{Se}$  (ICSD 150758) phase at low  $x$  value, corresponding to the  $\beta$ -phase of  $\text{Cu}_2\text{Se}$ . Based on the report on bulk  $\text{Cu}_{1.96}\text{S}_x\text{Se}_{1-x}$  by Mao et al.,<sup>[9]</sup> trigonal  $\text{Cu}_{2-y}\text{Se}$  was also expected, diminishing with increasing  $x$  with the appearance of hexagonal phase, although this cannot be observed from our data. We observe the trigonal  $\alpha$ - $\text{Cu}_{2-y}\text{Se}$  phase (ICSD 243952) at increased annealing temperatures, as described later. This behavior could possibly be attributed to the difference in fabrication and annealing strategies used for our thin film samples compared to bulk samples in the work by Mao et al. Yu et al.<sup>[28]</sup> claim that a high degree of Cu vacancies in  $\text{Cu}_{2-y}\text{Se}$  ( $y = 0.16 - 0.25$ ) gives predominantly  $\beta$ -phase, while more saturated samples are a mixture of  $\alpha$ -phase and  $\beta$ -phase. As the value of “ $y$ ” increases, the peak intensities corresponding to  $\alpha$ -phase should therefore gradually decrease. Although the phase evolution is the same, the mechanisms described in these two reports are conflicting, since increasing S content in the matrix is expected to decrease the number of Cu vacancies,<sup>[15]</sup> thereby increasing the Cu-saturation. In accordance with DFT calculations by Zhao et al.,<sup>[29]</sup> introducing S atoms into a Se site of  $\text{Cu}_2\text{Se}$  increases the bonding energy and the Cu vacancy formation energy, effectively fixing Cu atoms in the crystal lattice. We hypothesize that electrical conductivity measurements (presented later) should provide additional clarity in this case.

Scherrer analysis presented in Figure S1 and Table S1 in the SI shows that the grain size decreases with significantly increased S-content, as expected based on the size difference between S and Se atoms. However, no peak corresponding to the tetragonal  $\text{Cu}_2\text{S}$  phase can be observed in Figure S1, indicating that the crystal structure of  $\text{Cu}_{2-y}\text{Se}$  still dominates with the addition of S atoms up to  $x = 0.45 \pm 0.02$ , obtaining effective alloying with no phase separation occurring. This result stands in contrast to Ma et al.,<sup>[25]</sup> who mixed  $\text{Cu}_2\text{Se}$  and  $\text{Cu}_2\text{S}$  precursor inks and observed a predominant signal from the tetragonal  $\text{Cu}_2\text{S}$  phase for a S content of  $x = 0.48 \pm 0.048$ .

This observation indicates that the switch from predominantly alloyed  $\text{Cu}_2\text{SSe}$  mixtures to phase separated  $\text{Cu}_2\text{Se}$  and  $\text{Cu}_2\text{S}$  crystal structures might take place between  $x = 0.45$  and  $x = 0.48$  for  $\text{Cu}_{2-y}\text{S}_x\text{Se}_{1-x}$  direct thin films. While potentially interesting, phase separated thin films and their consequent thermoelectric properties will in general be hard to reproduce owing to variations in microstructure from batch to batch. Thus, we restrict our studies to sulfur content below 48%.

### Optical properties

Fig. 1 shows absorbance measurements for unsoaked (a) and Cu soaked (b)  $\text{Cu}_{2-y}\text{S}_x\text{Se}_{1-x}$  films with varying S content,  $x$ , annealed at 350 °C. It can be observed that the intraband absorption peak (between 1000 - 2500 nm) of unsoaked  $\text{Cu}_{2-y}\text{Se}$  is partially quenched by increased S substitution from 20 - 48% (Fig. 1a). This is due to increased copper-chalcogenide bond strength, restricting the formation of Cu vacancies as was predicted by Zhao et al.<sup>[15]</sup> Almost complete quenching of the intraband absorption is obtained through Cu soaking (Fig. 1b), as previously shown by us.<sup>[26]</sup> This is due to the significantly reduced number of Cu vacancies after soaking, restricting the excitation mechanism to interband only. Secondly, the interband transition slowly shifts to the blue with increased S concentration (Fig. 1b), indicating an increase in the band gap of the alloyed material which can be attributed to the higher bandgap of  $\text{Cu}_2\text{S}$  (1.2 eV) as compared to  $\text{Cu}_2\text{Se}$  (0.86 eV).<sup>[30,31]</sup> At the highest investigated S content, a peak/shoulder at ~800 nm indicative of  $\text{Cu}_2\text{S}$  appears for Cu soaked samples.<sup>[30]</sup>

### Thermoelectric performance

Fig. 2 shows improved thermoelectric performance at room temperature through Cu saturation and S substitution for  $\text{Cu}_{2-y}\text{S}_x\text{Se}_{1-x}$  films annealed at 350 °C. While the absolute values vary somewhat between sample batches, and Fig. 2 presents the samples with the highest performance - overall trends are the same, as illustrated by another representative sample batch (Figure S5 in SI). S:Se ratios from EDS measurements conducted using a Scanning Electron Microscope (SEM) indicate that residual S from EDT solvent remains ( $x = 0.16 \pm 0.016$ ) after annealing at 350 °C on a hot plate, even

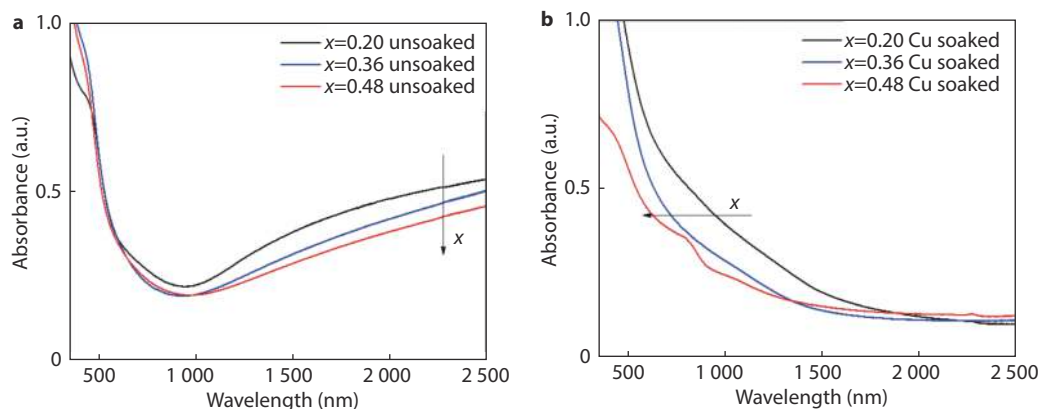


**Fig. 1** Room-temperature absorbance for unsoaked **a** and Cu soaked **b**  $\text{Cu}_{2-y}\text{S}_x\text{Se}_{1-x}$  ( $x = 0.20 \pm 0.019$ ,  $0.36 \pm 0.005$ ,  $0.48 \pm 0.032$ ) films annealed at 350 °C. Partial and full quenching of the high wavelength plasmon peak is observed both by S substitution and Cu saturation, respectively.

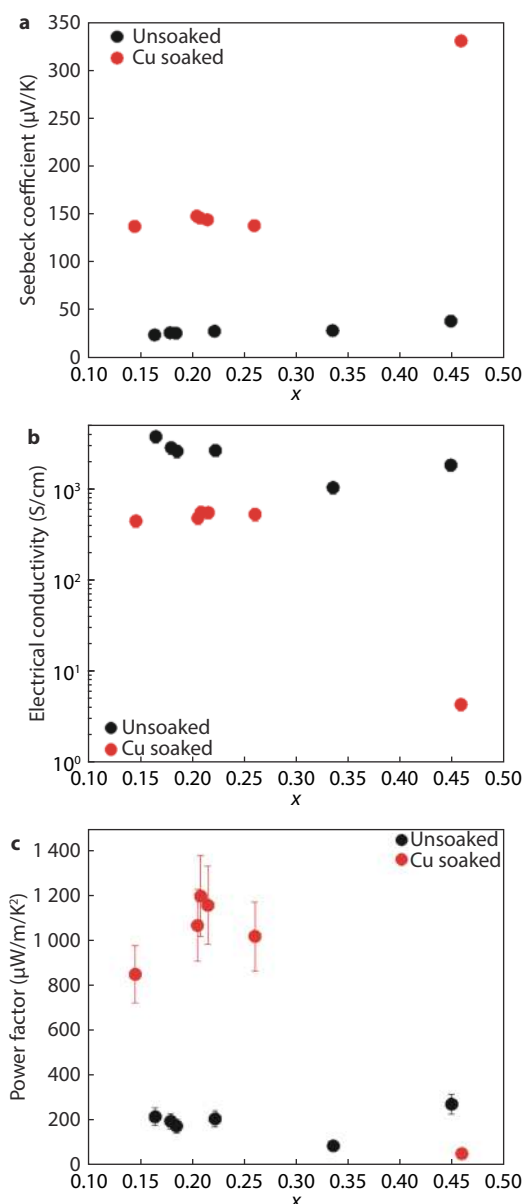


**Fig. 2** Thermoelectric properties of unsoaked (black) and Cu soaked (red)  $\text{Cu}_{2-y}\text{S}_x\text{Se}_{1-x}$  films annealed on hot plate at 350 °C as a function of S content, x. **a**, Seebeck coefficient as a function of S content before/after Cu soaking. A 5 – 7-fold increase in Seebeck coefficient is observed upon soaking as well as a slight increase upon increased S content. **b**, Electrical conductivity as a function of S content before/after Cu soaking. A significant decrease in electrical conductivity is observed after Cu soaking, and with increasing S content, especially for Cu soaked samples. Measurement uncertainties of electrical conductivity data were determined to ~15% and are captured within the data points. **c**, Power factor as a function of S content before/after 10 minutes soaking in 0.05 M Cu(I) in methanol. A 3 – 5-fold improvement of power factor is observed upon Cu soaking, except for x > 0.45. S substitution improves or sustains power factor up to x ~0.30 for soaked samples.

without extra S addition. Hence, we were unable to compare our data to pristine  $\text{Cu}_2\text{Se}$  following this protocol.

In Fig. 2a and 2b, it can be observed that the Seebeck coef-

ficient is improved 5 – 7-fold while the electrical conductivity is decreased by ~80% after Cu soaking up to x ~0.30. At even higher S content, x = 0.45, the Seebeck coefficient increase and the electrical conductivity decrease after soaking was even more dramatic. These observations can be explained by tuning of the carrier concentration, n, and effective carrier mass,  $m^*$ , affecting the Seebeck coefficient and electrical conductivity through equation (2) and (3), respectively:<sup>[3]</sup>

$$\alpha = \frac{8\pi^2 k_B^2}{3eh^2} m^* T \left( \frac{\pi}{3n} \right)^{2/3} \quad (2)$$

$$\sigma = ne\mu = \frac{n\tau e^2}{m^*} \quad (3)$$

where  $k_B$  is the Boltzmann constant, e is the electron charge, h is the Planck constant, T is temperature,  $\mu$  is the mobility and  $\tau$  is the carrier relaxation time.

When S is added to  $\text{Cu}_2\text{Se}$ , n is decreased due to the larger band gap of  $\text{Cu}_2\text{S}$  compared to  $\text{Cu}_2\text{Se}$ , as well as reduced intraband absorption (Fig. 1a). This results in a reduced free carrier concentration, increasing the Seebeck coefficient (Fig. 2a) and decreasing the electrical conductivity (Fig. 2b) with increasing x. Upon Cu soaking, Cu vacancies are filled, further reducing n, resulting in a significant shift in both Seebeck coefficient and electrical conductivity. The change in n with x causes less of a change in Seebeck coefficient and electrical conductivity at low x, but beyond x = 0.30 another significant shift in both parameters is observed. This signifies a large change in band gap, which can also be observed from the reduced absorption at x = 0.36 and x = 0.48 compared to x = 0.20 (Fig. 1b). The resulting power factors (Fig. 2c) show a 3 – 5-fold improvement after Cu soaking compared to unsoaked samples except at high levels of S substitution. The increased power factor upon Cu soaking is mainly due to the significant (5 – 7-fold) increase in the Seebeck coefficient, while the decreased power factor for x > ~0.30 in Cu soaked samples is mainly due to the significant decrease in electrical conductivity, as discussed above. S substitution increases or sustains power factors after soaking up to x ~0.30.

DFT calculations showed that in  $\text{Cu}_{2-y}\text{S}_x\text{Se}_{1-x}$ , both n and  $m^*$  exhibit non-monotonic (initially increasing, then decreasing) behavior with increasing S content, and the model correlated well with experimental data.<sup>[29]</sup> As discussed above, the addition of S atoms reduces n due to the larger band gap of  $\text{Cu}_2\text{S}$  compared to  $\text{Cu}_2\text{Se}$ , however the calculation showed that the non-monotonic Cu contribution with increasing x has a dominating effect on n. The S concentration dominates  $m^*$ . Since the Seebeck coefficient is proportional to  $m^* \left( \frac{1}{n} \right)^{2/3}$ , an increased Seebeck coefficient can be expected when the contribution of effective mass is stronger than the contribution from carrier density, while a decreasing trend can be expected in the opposite case. This indicates that the Seebeck coefficient is expected to go through a maximum at a certain S content. Similarly, the electrical conductivity ( $\sigma$ ) is proportional to  $\frac{n}{m^*}$ , as shown in equation (3), indicating an opposite trend compared to the Seebeck coefficient. However, the Zhao model disregards the average scattering time, which makes the prediction for electrical conductivity somewhat imprecise since presumably scattering increases due to doping/alloying. Additional scattering sources such as grain

boundaries in our nanostructures can also provide non-monotonous trends. Nevertheless, the resulting power factor,  $PF = \sigma\alpha^2$ , is expected to go through a maximum, which can be observed qualitatively for our Cu soaked samples at  $x = \sim 0.20$  (Fig. 2c).

### Seebeck coefficient stability

Fig. 3a shows the results of continuous measurement of the Seebeck coefficient for an unsoaked  $\text{Cu}_{2-y}\text{S}_x\text{Se}_{1-x}$  thin film with  $x = 0.16 \pm 0.02$  annealed at  $350^\circ\text{C}$  on a hot plate. The sample was exposed to a 15 K temperature gradient around room temperature in a nitrogen-filled glovebox with 60 seconds temperature equilibration time between subsequent measurement cycles. It can be observed that the Seebeck coefficient decreases with time over the entire 30-hour measurement span, with the rate of decrease governed by two different time constants. On a short time scale, below  $\sim 2$  hours (Zone I), the rate of decrease is much faster than for time scales above  $\sim 2$  hours (Zone II). The different regimes can be interpreted in accordance with Qiu et al.<sup>[11]</sup> (Fig. 3b): Mobile ions like  $\text{Cu}^+$  have high diffusivities due to low activation energies of migration in  $\text{Cu}_2\text{Se}$ . With no applied directional force or field, the ionic motion in the material is random. With an external driving force like a temperature gradient,  $\text{Cu}^+$  ions will start to flow in one direction, setting up a chemical concentration gradient inside the material. At the same time, reduction of  $\text{Cu}^+$  to Cu can occur at the cathode if the critical chemical potential is reached. We therefore hypothesize that, in Zone I,  $\text{Cu}^+$  ions are migrating to set up a concentration gradient as a response to the external field. In Zone II the concentration gradient has been established, and  $\text{Cu}^+$  ions are migrating to replenish reduced cations. The migration of  $\text{Cu}^+$  ions and subsequent reduction at the cathode leaves an increasing number of Cu vacancies, increasing the carrier concentration and decreasing the Seebeck coefficient in accordance with equation (2).

Increased Cu concentration in the proximity of the metal contacts (Cu:(Se+S) ratio  $\geq 2:1$ ) compared to in the center of the film (Cu:(Se+S) ratio 1.8:1) was observed by SEM-EDS (Figure S6 and S7 and Table S2 in SI). This supports the claim of a Cu concentration gradient in the sample after prolonged exposure to a temperature gradient. XPS data (Figure S8 in SI) identifies the presence of Cu, Se and S on the surface of a Cu soaked  $\text{Cu}_{2-y}\text{S}_x\text{Se}_{1-x}$  sample with  $x = 0.15$  after 117.5 h of continuous Seebeck measurements, but is inconclusive regarding the nature of Cu species being Cu(0) or Cu(I). LMM peaks from Auger Electron Spectroscopy could provide additional information to verify the presence of Cu(0) close to the metal contact, indicative of a reduction taking place in our thin films similar to what has been reported for bulk samples.<sup>[4,7]</sup> However, due to the successive reversal of the direction of the temperature gradient during our continuous Seebeck measurements, it might still be difficult to detect metallic Cu as the species would be oxidized upon reversal of the current flow.

Fig. 4 compares the results of continuous Seebeck coefficient measurements, as described above, for different scenarios. Fig. 4a-4b show the effect of Cu soaking for  $\text{Cu}_{2-y}\text{S}_x\text{Se}_{1-x}$  films with  $x = 0.15 - 0.16$  and  $x = 0.36$  annealed at  $350^\circ\text{C}$ . In both cases, Cu soaking decreases the stability of Seebeck

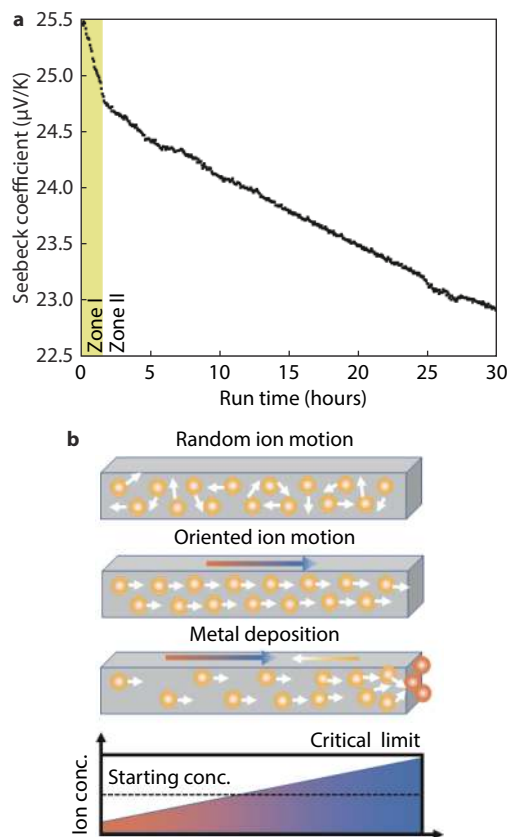


**Fig. 3** a, Continuous Seebeck coefficient measurement of unsoaked  $\text{Cu}_{2-y}\text{S}_x\text{Se}_{1-x}$  film annealed at  $350^\circ\text{C}$ , without the extra addition of S ( $x = 0.16 \pm 0.02$  due to contribution from EDT solvent). The Seebeck coefficient decreases following two mechanisms - on a short time scale,  $\sim 2$  hours (Zone I, yellow background), and at longer time scales (Zone II, white background). b, Schematic of random ion motion, oriented ion migration and metal deposition mechanism during thermoelectric device operation. Reproduced under terms of the CC-BY license.<sup>[11]</sup> Copyright 2018, Springer Nature.

coefficient over time, with a significant decrease in Seebeck coefficient of up to 20% in just 15 hours of operation. In comparison, for unsoaked samples the decrease during the first 15 hours of operation is limited to  $< 7\%$ . This is due to the thermodynamics of  $\text{Cu}_{2-y}\text{Se}$ , where the Cu deficient thin film is more thermodynamically stable than the Cu saturated thin film.<sup>[25,32]</sup> With a thermodynamic driving force to introduce vacancies, the carrier concentration increases with time and the Seebeck coefficient decreases following equation (2).

Fig. 4c-4d show the effect of sulfur for unsoaked and Cu soaked films annealed at  $350^\circ\text{C}$ . In both cases, Seebeck coefficient stability with time is improved by the addition of S. For Cu soaked samples, the decrease in Seebeck coefficient the first 15 hours of operation is reduced from 20% to 10% with increased S content from  $x = 0.15$  to  $x = 0.26$ . For unsoaked samples, a 5% decrease the first 8 hours of operation with  $x = 0.16$  is improved to a 2 % increase with  $x = 0.36$ . This is due to the increased bond strength when Se is replaced with S (14.2 meV per formula unit (f.u.) for  $n = 1$  in  $\text{Cu}_{64}\text{Se}_{32-n}\text{S}_n$ , 28.5 meV per f.u. for  $n = 2$ , 42.8 meV per f.u. for  $n = 3$ ),<sup>[15]</sup> increasing the barrier for  $\text{Cu}^+$  migration in the lattice. Additional stability

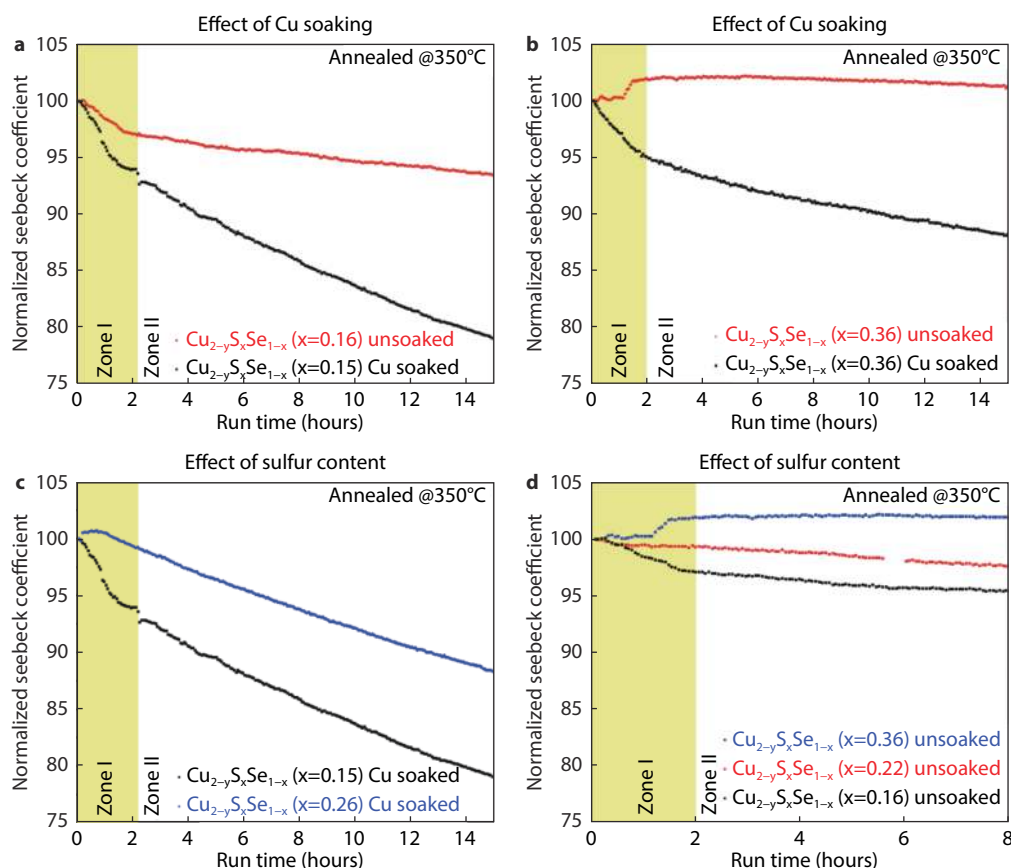


**Fig. 4** Stability of Seebeck coefficient over time. The yellow box indicates the period of initial degradation mechanism, Zone I. **a-b**, Effect of Cu soaking for films with  $x = 0.15 - 0.16$  and  $x = 0.36$  annealed at 350 °C: Cu soaking decreases Seebeck coefficient stability. **c-d**, Effect of sulfur for unsoaked and Cu soaked films annealed at 350 °C: addition of S improves Seebeck coefficient stability.

plots with calculated slopes can be found in the SI (Figure S9, S10 and S11).

### Improved Seebeck coefficient stability

Based on the presented results for  $\text{Cu}_{2-y}\text{S}_x\text{Se}_{1-x}$  films annealed at 350 °C, our approach to improve the performance and maintain high stability of the films was now to increase the annealing temperature. However, increasing the annealing temperature beyond 400 °C compromises the integrity of flexible polyimide (Kapton) substrates, thus establishing a critical boundary condition for our investigation. A series of unsoaked and Cu soaked films with different S contents were annealed in an oven at 400 °C, evaporating additional trapped solvent and exposing the films to a more uniform temperature treatment than annealing on the hot plate. The measured residual S content of  $x = 0.12 \pm 0.008$  for unsubstituted films with this treatment was slightly lower than unsubstituted films annealed at 350 °C ( $x = 0.16 \pm 0.016$ ).

Fig. 5 shows XRD spectra for unsaturated  $\text{Cu}_{2-y}\text{S}_x\text{Se}_{1-x}$  with  $x = 0.16 \pm 0.03$  annealed at different temperatures. At 350 °C, the cubic  $\beta\text{-Cu}_{2-y}\text{Se}$  phase is observed, as discussed in Section 3.1. With increasing temperature, a transition to the trigonal  $\alpha\text{-Cu}_{2-y}\text{Se}$  phase is observed. These observations are likely a Cu deficiency effect similar to what was observed by Scimeca et al.<sup>[26]</sup>, as chalcogens are expected to evaporate at increased annealing temperatures yielding a crystal structure with less Cu vacancies<sup>[25]</sup> and thus the trigonal structure is ex-

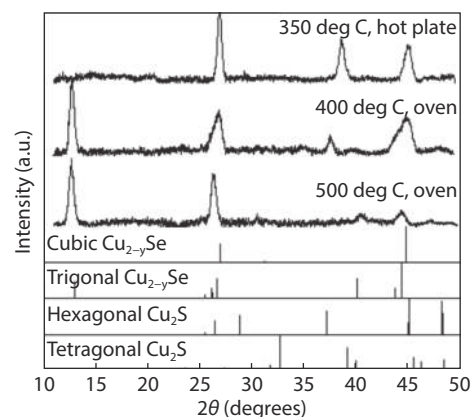


**Fig. 5** Room-temperature X-ray diffraction patterns for unsaturated  $\text{Cu}_{2-y}\text{S}_x\text{Se}_{1-x}$  ( $x = 0.16 \pm 0.03$ ) on glass annealed at different temperatures compared to reference spectra for cubic (ICSD 150758) and trigonal (ICSD 243952)  $\text{Cu}_{2-y}\text{Se}$ , and hexagonal (ICSD 95397) and tetragonal (ICSD 16550)  $\text{Cu}_{2-y}\text{S}$ , respectively. The samples underwent thermoelectric characterization prior to XRD characterization. The trigonal  $\text{Cu}_{2-y}\text{Se}$  phase appears with increasing annealing temperature. The origin of the peaks at  $2\theta \sim 38$  is likely diffusion of metal ions from the gold contacts, however this is currently still under investigation.

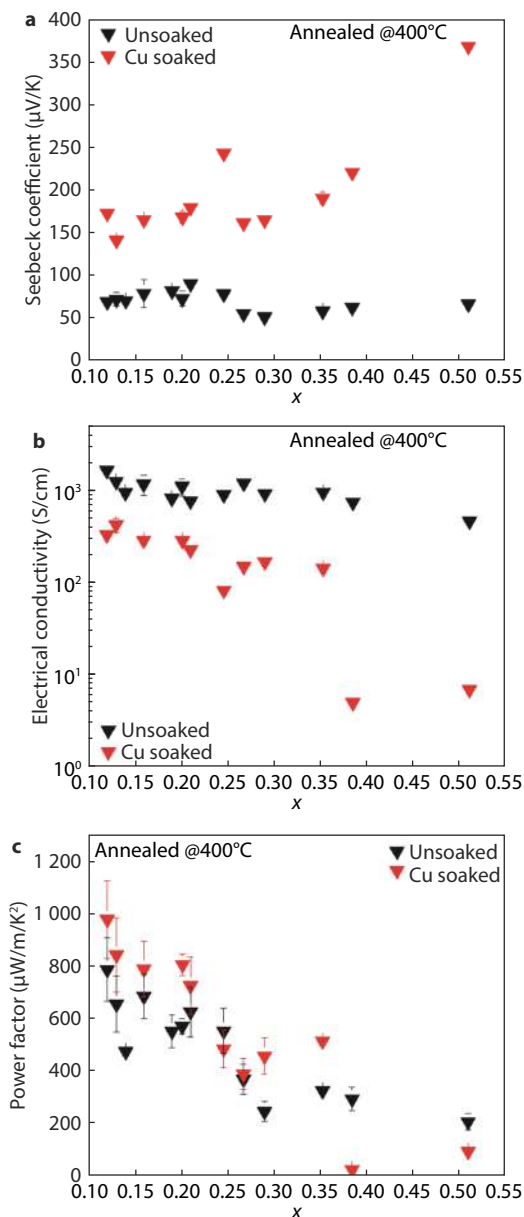
pected. The origin of the peaks at  $2\theta \sim 38$  is unclear and is currently under investigation, as discussed in the SI, however likely due to diffusion of metallic gold atoms from contacts applied to perform thermoelectric characterization.

Fig. 6 shows significantly improved thermoelectric performance (up to 300% improved power factor at  $x < \sim 0.15$ ) of unsoaked  $\text{Cu}_{2-y}\text{S}_x\text{Se}_{1-x}$  films with  $x < 0.30$  annealed in an oven at  $400^\circ\text{C}$  compared to films annealed on a hot plate at  $350^\circ\text{C}$  (Fig. 2). This is due to a reduced number of Cu vacancies with increasing annealing temperature,<sup>[25]</sup> as manifested through an increased Seebeck coefficient (Fig. 6a) and slightly reduced electrical conductivity (Fig. 6b). The effect on  $\alpha$  and  $\sigma$  by  $n$  (and  $m^*$ ) can be interpreted through equation (2) and (3), as thoroughly discussed in Section 3.3. Additional data points for films annealed at  $400^\circ\text{C}$  are presented in the SI (Figure S12). Figure S13 directly compares Seebeck coefficients, electrical conductivities and resulting power factors for unsoaked and Cu soaked films annealed at  $350^\circ\text{C}$  and  $400^\circ\text{C}$ .

The room temperature power factors of films annealed at  $400^\circ\text{C}$  (Fig. 6c) increased marginally with Cu soaking, and decreased with increasing S substitution for both unsoaked and Cu soaked samples. The observed change with Cu soaking and varying  $x$  is due to the combined contribution of 3-fold improvement of Seebeck coefficient and significant reduction of electrical conductivity after Cu soaking, in addition to a negative effect on electrical conductivity by increasing S content.

Since the power factor of films annealed at  $400^\circ\text{C}$  was only marginally improved through Cu soaking, the highest power factors in this investigation were obtained with Cu soaked films annealed at  $350^\circ\text{C}$ . This result is important because as we have observed in Fig. 4a–4b and as observed by Scimeca et al.,<sup>[26]</sup> while Cu-soaking increases power factors, the improvement comes at the expense of reduced stability. Fig. 7 shows the effect of annealing temperature for unsoaked films with  $x = 0.14 - 0.16$ . The Seebeck coefficient stability the first 15 hours is increased by nearly 5% when annealing at  $400^\circ\text{C}$  instead of  $350^\circ\text{C}$ . Operating at slightly higher temperatures than room temperature does not significantly affect the stability of these samples, as visualized in Fig. 7b. Additional Seebeck measurements at slightly higher temperatures are shown in SI Figure S14 and Figure S15.

Notably, the film annealed at  $400^\circ\text{C}$  has a 3-fold higher absolute Seebeck coefficient than the sample annealed at  $350^\circ\text{C}$  (Figure S13a in SI). This is in line with Ma et al.<sup>[25]</sup> who reported that when the annealing temperature of  $\text{Cu}_{2-y}\text{S}_x\text{Se}_{1-x}$  films was increased, the number of Cu vacancies were reduced due to the loss of chalcogen with higher annealing temperature. However, this seems to affect the Seebeck stability differently than in the case when Cu vacancies are reduced due to Cu soaking, which caused less stable performance (Fig. 4a and 4b). We hypothesize that, due to the strength of the bonds formed, filling vacancies with external  $\text{Cu}^+$  ions at room temperature establishes a less stable stoichiometric equilibrium than approaching stoichiometric balance by removal of chalcogens at high temperature. These secondary Cu-Se bonds, formed asynchronously with respect to the primary Cu-Se bonds in the original crystal structure, can be imagined to rely on less ideal coordination as the ions are forced to occupy an existing vacancy at room temperat-



**Fig. 6** Average thermoelectric properties of unsoaked (black) and Cu soaked (red)  $\text{Cu}_{2-y}\text{S}_x\text{Se}_{1-x}$  films annealed in an oven at  $400^\circ\text{C}$  as a function of S content,  $x$ . Standard deviations for y-values are shown as error bars where appropriate. Standard deviations for x-values are generally captured within the data points. The full data sets are shown in the SI (Figure S12). **a**, Seebeck coefficient. A 3-fold increase in Seebeck coefficient upon Cu soaking compared to the unsoaked sample is observed. The Seebeck coefficient of Cu soaked samples increases slightly with S content up to  $x \sim 0.40$ . **b**, Electrical conductivity. A significant reduction in electrical conductivity is observed upon Cu soaking. Electrical conductivity decreases slightly with increasing S content. **c**, Power factor. The power factor increases 20 - 50% after 10 min soaking in 0.05 M Cu(I) in methanol compared to before soaking for  $x$  up to  $\sim 0.35$ . A decreasing trend in power factor with increasing  $x$  is observed for both unsoaked and Cu soaked samples. The S content in unsoaked samples is estimated based on the S content in the corresponding Cu soaked sample.

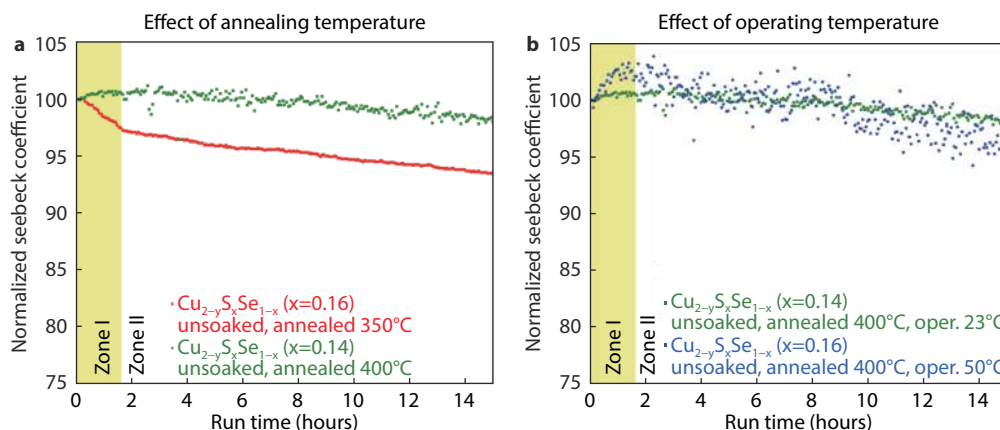


**Fig. 7** Stability of Seebeck coefficient over time. The yellow box indicates the period of initial degradation mechanism, Zone I. **a**, Effect of annealing temperature for unsoaked films with  $x = 0.14 - 0.16$ : Increased Seebeck coefficient stability after annealing at 400 °C. **b**, Effect of operating temperature for unsoaked films with  $x = 0.14 - 0.16$ : Slightly reduced Seebeck coefficient stability at 50 °C compared to 23 °C.

ure. Thus, annealing at increased temperature results in higher stability.

With the improvements observed annealing the films at 400 °C, a logical next step would be to investigate even higher annealing temperatures. Some preliminary results for  $\text{Cu}_{2-y}\text{S}_x\text{Se}_{1-x}$  films annealed at 450 °C and 500 °C are shown in the SI (Figure S16 and S17) as well as in the work by Lin et al.<sup>[23]</sup> However, as discussed previously, these annealing temperatures are not generally compatible with flexible substrates.

Table 1 compares the power factors obtained in this work with power factors for other reported solution processed thin films and bulk samples. Albeit unstable, we report Cu soaked  $\text{Cu}_{2-y}\text{S}_x\text{Se}_{1-x}$  thin films annealed at 350 °C with comparable performance to bulk  $\text{Cu}_2\text{S}_x\text{Se}_{1-x}$  at room temperature. More importantly, with unsoaked  $\text{Cu}_{2-y}\text{S}_x\text{Se}_{1-x}$  thin films annealed at 400 °C we are demonstrating optimal stability (~5% less degradation of Seebeck coefficient after 15 hours compared to Scimeca et al.<sup>[26]</sup>) and record power factors of  $\sim 800 \mu\text{W m}^{-1} \text{K}^{-2}$  at room temperature. This is much higher than the performance of  $\text{Cu}_{2-y}\text{S}_x\text{Se}_{1-x}$  films obtained through any other facile solution processed route and on par with bulk samples.

## Conclusion

In this work we have shown that the thermoelectric properties of liquid-like  $\text{Cu}_{2-y}\text{S}_x\text{Se}_{1-x}$  can be tuned and stabilized by optimization of the Cu and S contents as well as annealing temperature.  $\text{Cu}_{2-y}\text{S}_x\text{Se}_{1-x}$  direct thin films were fabricated from a solution-based route and characterized through an array of techniques. The cubic  $\text{Cu}_2\text{ySe}$  crystal structure was preserved with increasing S content up to  $x \sim 45\%$ . Quenching of the intra-band absorption peak was observed with increased S content and Cu saturation, which demonstrates that the carrier concentration was reduced. Thermoelectric measurements showed up to a 5.5-fold increase in power factor with Cu saturation, from  $204 \mu\text{W m}^{-1} \text{K}^{-2}$  to  $1156 \mu\text{W m}^{-1} \text{K}^{-2}$  for 22% sulfur, and an increased or sustained power factor up to a S content up to  $\sim 30\%$  for saturated films annealed at 350 °C. Continuous Seebeck coefficient measurements revealed a decrease with time following two different regimes related to the migration of Cu ions as a response to an external temper-

ature gradient. We verified that the Seebeck coefficient stability in direct thin films is improved with the addition of S, while Cu saturation, although beneficial to the power factor, results in a more rapid degradation of the Seebeck coefficient. We showed that by increasing the annealing temperature to 400 °C, record room temperature power factors of  $\sim 800 \mu\text{W m}^{-1} \text{K}^{-2}$  could be obtained with  $\sim 15\%$  sulfur content without Cu soaking, while simultaneously improving the stability by  $\sim 5\%$ . The direct thin film route proved suitable for tuning the carrier concentration in  $\text{Cu}_{2-y}\text{S}_x\text{Se}_{1-x}$  in order to fabricate films with increased performance stability, supporting the case for  $\text{Cu}_{2-y}\text{S}_x\text{Se}_{1-x}$  direct thin films as a heavy metal-free alternative for scavenging low grade waste heat at room temperature. Our results demonstrate that by introducing isovalent impurities and optimizing the annealing temperature, it is possible to improve the stability of  $\text{Cu}_{2-y}\text{Se}$  thin films while maintaining high thermoelectric performance on par with bulk samples.

## ACKNOWLEDGEMENTS

The authors acknowledge the use of shared facilities provided through the Materials Research Science and Engineering Center (MRSEC) program of the National Science Foundation under Award Numbers DMR-1420073 and DMR-0923251.

This work was performed in part at the Advanced Science Research Center NanoFabrication Facility of the Graduate Center at the City University of New York.

## CONFLICTS OF INTEREST

The authors declare no conflicts of interest.

## AUTHOR CONTRIBUTIONS

Conceptualization: A.S.; Data Curation: A.S., H.M.; Formal Analysis: H.M.; Funding Acquisition: A.S.; Investigation: H.M., M.R.S.; Methodology: A.S.; Project Administration: A.S.; Resources: H.M.; Supervision: A.S.; Validation: A.S., H.M., M.R.S.; Visualization: H.M.; Writing-Original Draft: H.M.; Writing-Review & Editing: A.S., H.M., M.R.S.

**Table 1.** Reported thermoelectric performance  $\text{Cu}_{2-y}\text{S}_x\text{Se}_{1-x}$ 

Fabrication technique	Temperature [K]	Power factor $\text{Cu}_{2-y}\text{Se}$ [ $\mu\text{W m}^{-2}\text{K}^{-2}$ ]	Power factor $\text{Cu}_2\text{Se}$ [ $\mu\text{W m}^{-2}\text{K}^{-2}$ ]	Power factor $\text{Cu}_{2-y}\text{S}_x\text{Se}_{1-x}$ [ $\mu\text{W m}^{-2}\text{K}^{-2}$ ]	Power factor $\text{Cu}_2\text{S}_x\text{Se}_{1-x}$ [ $\mu\text{W m}^{-2}\text{K}^{-2}$ ]	Ref.
Solution processed	300	100 - 200	-	-	-	[23]
Solution processed	300	~175	653	-	-	[26]
Solution processed	300	-	-	97.8 ( $x = 0.31$ )	-	[25]
Solution processed	300	~125	-	120 ( $x = 0.48$ )	-	[27]
Ball milled & printed	300	50	-	250 ( $x = 0.10$ )	-	[22]
High-pressure, high-temperature	300	-	400	-	450 ( $x = 0.01$ )	[33]
High-pressure, high-temperature	325	-	-	~450 ( $x = 0.8, y = 0.2$ )	540 ( $x = 0.03$ )	[18]
Mechanical alloying & spark plasma sintering	325	-	600	-	270 - 490 (15 - 5 wt% $\text{Cu}_2\text{S}$ )	[12]
Mechanical alloying & spark plasma sintering	300	-	-	-	140 ( $x = 0.85$ )	[34]
Mechanical alloying & spark plasma sintering	325	-	-	~100 ( $y = 0.2$ )	50 ( $x = 1$ )	[35]
Melting- annealing	340	700 - 850	750	-	-	[6]
Melting- annealing	300	600	700	450 - 650	800 - 1000	[9]
Melting- annealing	300	-	750	~200 ( $x = 0.50$ )	775 - 1125 ( $x < 0.20$ )	[15-17]
Pulsed laser deposition	325	844	-	-	-	[20]
Wet-chemical synthesis, vacuum assisted filtration + cold pressing	300	270 <sup>a)</sup>	-	-	-	[21]
Pulsed hybrid reactive magnetron sputtering	300	200 - 900	1100	-	-	[19]
Solution processed (This work)	300	-	-	200 ( $T_{\text{ann}} 350^\circ\text{C}$ , $x < 0.20$ )	847 - 1196 ( $T_{\text{ann}} 350^\circ\text{C}$ , $x < 0.30$ )	This work
				800 ( $T_{\text{ann}} 400^\circ\text{C}$ , $x < 0.15$ )		

<sup>a)</sup>Composite PEDOT: PSS coated polycrystal  $\text{Cu}_x\text{Se}_y$  nanowire films with Cu: Se ratio of 3

## REFERENCES

- H. Ritchie and M. Roser (2021) - Energy. Published in Our World in Data. Online at: <https://ourworldindata.org/energy>
- M. M. Kostic, *Encyclopedia of Energy Engineering*, Vol. II (Eds: S. Anwar), Taylor & Francis Group, USA, 2014, Ch. "Energy: Global and Historical Background".
- G. J. Snyder and E. S. Toberer, *Nat. Mater.*, 2008, 7, 105
- Z. Zhang, K. Zhao, T.-R. Wei, P. Qiu, L. Chen and X. Shi, *Energy Environ. Sci.*, 2020, 13, 3307
- H. Liu, X. Shi, F. Xu, L. Zhang, W. Zhang, L. Chen, Q. Li, C. Uher, T. Day and G. J. Snyder, *Nat. Mater.*, 2012, 11, 422
- D. Yang, X. Su, J. Li, H. Bai, S. Wang, Z. Li, H. Tang, K. Tang, T. Luo, Y. Yan, J. Wu, J. Yang, Q. Zhang, C. Uher, M. G. Kanatzidis and X. Tang, *Adv. Mater.*, 2020, 32, 2003730
- W.-D. Liu, L. Yang and Z.-G. Chen, *Nano Today*, 2020, 35, 100938
- G. Li, G. Song, N. Wang, F. Hu, Y. Wu, H. Du and J. Yuo, *Surf. Interfaces*, 2022, 28, 101651
- T. Mao, P. Qiu, X. Du, P. Hu, K. Zhao, J. Xiao, X. Shi and L. Chen, *Adv. Funct. Mater.*, 2020, 30, 1908315
- G. Dennler, R. Chmielowski, S. Jacob, F. Capet, P. Roussel, S. Zastrow, K. Nielsch, I. Opahle and G. K. H. Madsen, *Adv. Energy Mater.*, 2014, 4, 1301581
- P. Qiu, M. T. Agne, Y. Liu, Y. Zhu, H. Chen, T. Mao, J. Yang, W. Zhang, S. M. Haile, W. G. Zeier, J. Janek, C. Uher, X. Shi, L. Chen and G. J. Snyder, *Nat. Commun.*, 2018, 9, 2910
- M. U. Farooq, S. Butt, K. Gao, X. Sun, X. Pang, S. U. Khan, W. Xu, F. Mohamed, A. Mahmood and N. Mahmood, *Ceram. Int.*, 2016, 42, 8395
- T. P. Bailey, S. Hui, H. Xie, A. Olvera, P. F. P. Poudeu, X. Tang and C. Uher, *J. Mater. Chem. A*, 2016, 4, 17225
- S. D. Kang, J.-H. Pöhls, U. Aydemir, P. Qiu, C. C. Stoumpos, R. Hanus, M. A. White, X. Shi, L. Chen, M. G. Kanatzidis and G. J. Snyder, *Mater. Today Phys.*, 2017, 1, 7
- K. Zhao, A. B. Blichfeld, H. Chen, Q. Song, T. Zhang, C. Zhu, D. Ren, R. Hanus, P. Qiu, B. B. Iversen, F. Xu, G. J. Snyder, X. Shi and L. Chen, *Chem. Mater.*, 2017, 29, 6367
- K. Zhao, A. B. Blichfeld, E. Eikeland, P. Qiu, D. Ren, B. B. Iversen, X.

- Shi and L. Chen, *J. Mater. Chem. A*, 2017, 5, 18148
17. K. Zhao, P. Qiu, Q. Song, A. B. Blichfeld, E. Eikeland, D. Ren, B. Ge, B. B. Iversen, X. Shi and L. Chen, *Mater. Today Phys.*, 2017, 1, 14
  18. S. Xiang, Y. Liang, M. Zhou and X. Zhang, *J. Alloys Compd.*, 2022, 910, 164812
  19. J. A. Perez-Taborda, L. Vera, O. Caballero-Calero, E. O. Lopez, J. J. Romero, D. G. Stroppa, F. Briones and M. Martin-Gonzalez, *Adv. Mater. Technol.*, 2017, 2, 1700012
  20. A. Wang, Y. Xue, J. Wang, X. Yang, J. Wang, Z. Li and S. Wang, *Mater. Today Energy*, 2022, 24, 100929
  21. Y. Lu, Y. Ding, Y. Qiu, K. Cai, Q. Yao, H. Song, L. Tong, J. He and L. Chen, *ACS Appl. Mater. Interfaces*, 2019, 11, 12819
  22. M. M. Mallick, A. Sarbajna, A. G. Rösch, L. Franke, H. Geßwein, Y. M. Eggeler and U. Lemmer, *Appl. Mater. Today*, 2022, 26, 101269
  23. Z. Lin, C. Hollar, J. S. Kang, A. Yin, Y. Wang, H.-Y. Shiu, Y. Huang, Y. Hu, Y. Zhang and X. Duan, *Adv. Mater.*, 2017, 29, 1606662
  24. D. H. Webber and R. L. Brutchey, *J. Am. Chem. Soc.*, 2013, 135, 15722
  25. Y. Ma, P. B. Vartak, P. Nagaraj and R. Y. Wang, *RSC Adv.*, 2016, 6, 99905
  26. M. R. Scimeca, F. Yang, E. Zaia, N. Chen, P. Zhao, M. P. Gordon, J. D. Forster, Y.-S. Liu, J. Guo, J. J. Urban and A. Sahu, *ACS Appl. Energy Mater.*, 2019, 2, 1517
  27. N. Chen, M. R. Scimeca, S. J. Paul, S. B. Hafiz, Z. Yang, X. Liu, F. Yang, D.-K. Ko and A. Sahu, *Nanoscale Adv.*, 2020, 2, 368
  28. J. Yu, K. Zhao, P. Qiu, X. Shi and L. Chen, *Ceram. Int.*, 2017, 43, 11142
  29. L. Zhao, F. Y. Fei, J. Wang, F. Wang, C. Wang, J. Li, J. Wang, Z. Cheng, S. Dou and X. Wang, *Sci. Rep.*, 2017, 7, 40436
  30. S. C. Riha, R. D. Schaller, D. J. Gosztola, G. P. Wiederrecht and A. B. F. Martinson, *J. Phys. Chem. Lett.*, 2014, 5, 4055
  31. J.-H. Choi and Y.-K. Han, *Curr. Appl. Phys.*, 2015, 15, 1417
  32. J. D. Forster, J. J. Lynch, N. E. Coates, J. Liu, H. Jang, E. Zaia, M. P. Gordon, M. Szybowski, A. Sahu, D. G. Cahill and J. J. Urban, *Sci. Rep.*, 2017, 7, 2765
  33. L. Xue, C. Fang, W. Shen, M. Shen, W. Ji, Y. Zhang, Z. Zhang and X. Jia, *Mod. Phys. Lett. B*, 2020, 34, 2050006
  34. Y. Yao, B.-P. Zhang, J. Pei, Y.-C. Liu and J.-F. Li, *J. Mater. Chem. C*, 2017, 5, 7845
  35. Y.-H. Ji, Z.-H. Ge, Z. Li and J. Feng, *J. Alloys Compd.*, 2016, 680, 273



©2023 The Authors. *Materials Lab* is published by Lab Academic Press. This is an open access article under the terms of the Creative Commons Attribution License, which permits use, distribution and reproduction in any medium, provided the original work is properly cited.